Res Chem Intermed (2015) 41:7449–7461
DOI 10.1007/s11164-014-1836-x

Ultrasonic-assisted synthesis of visible-light-driven TiO_2/Bi_2O_3 nanocomposite photocatalysts: characterization, properties and azo dye removal application

Liang An · Guanghui Wang · Yang Cheng · Lei Zhao · Fang Gao · Yongsheng Tian

Received: 27 May 2014 / Accepted: 24 September 2014 / Published online: 12 October 2014

Abstract TiO_2/Bi_2O_3 nanocomposites (Sonic-TiO_2/Bi_2O_3) were synthesized via combination of thermohydrolysis and ultrasonic chemical precipitation techniques. For the sake of contrast, pure TiO_2 nanoparticles (NPs) and conventional TiO_2/Bi_2O_3 nanocomposites (Stir-TiO_2/Bi_2O_3) were also prepared. XRD, FT-IR, FE-SEM, TEM, EDX and UV–Vis studies were adopted to determine the structural, chemical composition and optical properties of the as-prepared samples. The photocatalytic activities of the samples were evaluated by measuring the photo-degradation of Orange II in aqueous solution under visible light irradiation ($\lambda \geq 400$ nm). The efficiencies towards OII degradation were determined to be 44.0, 81.8 and 94.7 % for pure TiO_2 NPs, Stir-TiO_2/Bi_2O_3 and Sonic-TiO_2/Bi_2O_3, respectively. These results reveal that the loading of Bi_2O_3 can greatly improve visible light photocatalytic performance of TiO_2, and the ultrasonic treatment can also improve photocatalytic performance of TiO_2/Bi_2O_3 nanocomposites. Based on the experimental results, possible enhanced visible-light photocatalytic degradation mechanisms were also discussed. The present findings may provide a new approach to synthesize high efficiency TiO_2/Bi_2O_3 nanocomposite photocatalysts.

Keywords TiO_2 · Bi_2O_3 · Nanocomposites · Ultrasonic · Photocatalysis

Introduction

With the development of the chemical industry, more and more chemicals have been synthesized and used on many occasions. As a result, more and more

L. An · G. Wang (✉) · Y. Cheng · L. Zhao · F. Gao · Y. Tian
College of Chemical Engineering and Technology, Wuhan University of Science and Technology, Wuhan 430081, People's Republic of China
e-mail: onion7891@163.com

poisonous waste water containing organic pollutants has been produced [1]. In almost all countries of the world, the poisonous organic waste water needs to be treated to remove the organic pollutants before being discharged [2]. Various methods such as absorption [3], ultrasonic degradation [4], biodegradation [5] and photocatalysis [6] have been used to reach this goal. Among these methods, photocatalysis has been regarded as one of the most promising sewage treatment techniques due to its low cost and non-toxic and efficiency natures [7].

Up to the present, much research has proved that photocatalysis is an effective method of destroying organic aqueous waste streams [8]. Unfortunately, the photocatalysis technique still has many problems, which restrict its large-scale industrial application [9]. For example, most of the high efficiency photocatalysts like TiO_2 (band gap = 3.2 eV), ZnO (band gap = 3.2 eV) and so on are wide gap semiconductors: they can only be activated by UV light, which is a very small proportion of sunlight [10]. In order to harness the cheap and clean sunlight power efficiently, it is necessary to develop new visible light (45 % of the solar spectrum)-activated photocatalysts with narrow band gap and high catalytic capability [11].

Bi_2O_3, a narrow band gap (band gap = 2.8 eV) semiconductor, has attracted much attention due to its unique optical and electrical properties [12]. Many research groups have investigated the photocatalytic performance of Bi_2O_3, and the results show that the Bi_2O_3 can exhibit photocatalytic activities [13]. Unfortunately, pure Bi_2O_3 cannot be used as an efficient visible light-driven photocatalyst because of its low photocatalytic performance. To solve this problem, three principal kinds of modification methods have been developed. The first method is the doping of new elements [14], the second is the loading of precious metals [15], and the last is modification with semiconductors; for example, when Bi_2O_3 was combined with TiO_2, a wide band gap semiconductor, the as-prepared nanocomposite materials exhibited excellent photocatalytic performances under visible light irradiation, even better than pure TiO_2 and Bi_2O_3 [16, 17]. Therefore, the TiO_2/Bi_2O_3 nanocomposite materials can be regarded as a promising candidate for the new visible light-driven activated photocatalysts which we want.

Currently, several methods have been developed for the synthesis of TiO_2/Bi_2O_3 nanocomposite materials. Huo et al. [18] have prepared ordered TiO_2/Bi_2O_3 film by the sol–gel method in a presence template. Li et al. [19] have fabricated heterostructured TiO_2/Bi_2O_3 composite fibers via combination of the solvothermal method and electrospinning technique. In addition, the electrochemical anode method [20], the evaporation-induced self-assembly method [21] and the blending method [22] have also been applied in the synthesis of TiO_2/Bi_2O_3 nanocomposite materials. Although the preparation and photocatalytic performances of TiO_2/Bi_2O_3 nanocomposite materials have been reported many times over the years, most of them employ traditional synthetic methods. Research on ultrasonic-assisted synthesis of these materials has seldom been reported. In this work, sonochemical synthesis, a new synthetic method compared to the general methods, has been applied in the preparation of TiO_2/Bi_2O_3 nanocomposites, and we hope we can obtain a new highly efficient TiO_2/Bi_2O_3 nanocomposite photocatalyst.

TiO_2/Bi_2O_3 nanocomposites (Sonic-TiO_2/Bi_2O_3) were prepared via the combination of the hermohydrolysis method and the ultrasonic-assisted chemical

precipitation technique. For comparison, pure TiO_2 nanoparticles (NPs) and conventional TiO_2/Bi_2O_3 nanocomposites (Stir-TiO_2/Bi_2O_3) were also prepared. All the as-synthesized products were well characterized with the aid of X-ray diffraction (XRD), Fourier transform-infrared spectroscopy (FT-IR), field-emission scanning electron microscopy (FE-SEM), transmission electron microscopy (TEM), energy dispersive analysis of X-ray (EDX) and ultra-violet adsorption spectrum (UV–Vis). The photocatalytic activities of all the samples have also been investigated by the photocatalytic decolorization of Orange II (OII) in aqueous solution under visible light irradiation.

Experimental

Materials

Chemicals used in the experiment were titanium oxysulfate hydrate ($TiOSO_4 \cdot xH_2O$, CP), bismuth nitrate pentahydrate ($Bi(NO_3)_3 \cdot 5H_2O$, AR), hexamethylene-tetramine (HMT, $C_6H_{12}N_4$, AR), ethylene glycol (EG, $C_2H_6O_2$, AR) and orange II (OII, $C_{16}H_{11}N_2NaO_4S \cdot 5H_2O$, AR). $TiOSO_4 \cdot xH_2O$ was purchased from Tianjin Guangfu Fine Chemical Research Institute (Tianjin, PR China), and the others were all purchased from Sinopharm Chemical Reagent (Shanghai, PR China). All the reagents were used without further purification. Deionized water used throughout the experiments was prepared from a laboratory ultra-pure water purifier.

Preparation of TiO_2 nanoparticles with the thermohydrolysis method

The TiO_2 NPs were synthesized via the thermohydrolysis technique [23]. Typically, 10 g of $TiOSO_4 \cdot xH_2O$ were added to 45 mL of distilled water at room temperature under continuous stirring. After being stirred for more 30 min, the mixture was transferred into a Teflon-lined stainless-steel autoclave (100 mL capacity) and sealed. After being heated at 100 °C for 48 h, the autoclave was cooled to room temperature. The white precipitates were collected, washed, and then dried in an oven at 80 °C for 6 h. Next, the obtained white powders were annealed at 600 °C for 6 h, and then well-crystallized TiO_2 NPs were obtained.

Preparation of TiO_2/Bi_2O_3 nanocomposites with ultrasonic-assisted chemical precipitation method

In a typical case, 1.6 g of TiO_2 NPs were dispersed in 50 mL $Bi(NO_3)_3$ EG solution (0.04 mol/L) to form a white suspension under vigorous stirring, and then 50 mL of the HMT EG solution (0.04 mol/L) were poured into the above suspension. The obtained mixture was transferred to a conical flask and heated at boiling temperature until all the EG had evaporated, while an ultrasonic bath (40 kHz, 120 W; NingBo Scientz Biotechnology, PR China) was applied to treat the mixture in this heating process. After that, the product was collected and calcined at 300 °C for 4 h. Finally, the TiO_2/Bi_2O_3 nanocomposites (denoted by Sonic-TiO_2/Bi_2O_3) were

obtained, and the nominal weight fraction of Bi_2O_3 to $Bi_2O_3 + TiO_2$ in the Sonic-TiO_2/Bi_2O_3 was about 36.8 %.

Preparation of TiO_2/Bi_2O_3 nanocomposites with conventional precipitation method

To investigate the influence of ultrasonic treatment on the chemical constitution, morphologies, optical properties and photocatalytic performances of Sonic-TiO_2/Bi_2O_3 nanocomposites, another kind of TiO_2/Bi_2O_3 nanocomposite materials were synthesized by a conventional precipitation method. In the conventional preparation process, the ultrasonic treatment was replaced by vigorous stirring, while the other procedures were all the same compared with the synthesis process of Sonic-TiO_2/Bi_2O_3 nanocomposites. The as-obtained sample was called Stir-TiO_2/Bi_2O_3, and the nominal weight fraction of Bi_2O_3 to $Bi_2O_3 + TiO_2$ in the Stir-TiO_2/Bi_2O_3 was the same as that in the Sonic-TiO_2/Bi_2O_3.

Characterization

All the three prepared samples (TiO_2 NPs, Sonic-TiO_2/Bi_2O_3 and Stir-TiO_2/Bi_2O_3) were analyzed for their crystallite phase with a X-ray diffractometer (XRD, X'Pert PRO; Philips, Netherlands) with Cu Kα radiation ($\lambda = 1.5418$ Å). Jade software was also used for the analysis of different peaks. The functional groups of the samples were examined through a Fourier transform-infrared spectroscopy (FT-IR, NEXUS-6700; Nicolet, USA) using a KBr pressed disk. The morphologies and element distribution of them were characterized by field emission scanning electron microscopy (FE-SEM, Nova 400 Nano; FEI, America) with energy-dispersive spectra (EDX, IE 350 Penta FET X-3; Oxford Inca, UK) and transmission electron microscopy (TEM, Tecnai G20; FEI). The optical absorption properties were performed using a UV–Visible absorption spectrometer (UV–Vis, U-3010; HITACHI, Japan). Furthermore, the absorbance of dye solution in photocatalytic experiments was measured with a visible spectrophotometer (V-1600; MAPADA, China).

Photocatalysis experiment

Photocatalytic activities of the samples were evaluated by the degradation of OII under visible light with a home-made photocatalytic reaction system. A 500-W halogen tungsten lamp (Philips) equipped with a cutoff filter ($\lambda \geq 400$ nm) was employed as the visible light source, and a magnetic stirrer was also applied to agitate the suspension containing the photocatalysts and dye solution. To keep a uniform temperature, the suspension of photocatalysts and OII solution was cooled with a constant temperature water bath.

In a typical photocatalytic test, 0.15 g of Sonic-TiO_2/Bi_2O_3 were suspended in 150 mL OII aqueous solution (5 mg/L) and stirred for 30 min in the dark to ensure that the OII molecules absorbed completely on the catalyst surface before irradiation. Then, the light was turned on and the photocatalytic reactions started.

Under stirring, about 5 mL of suspension was taken out at regular intervals of 30 min, centrifuged, and analyzed using a visible light spectrophotometer. The photocatalytic efficiency (E) was evaluated in terms of the percentage of OII degraded using the following equation:

$$E(\%) = \frac{C_0 - C}{C_0} \times 100 \quad (1)$$

where C_0 (mg/L) is the initial concentration of OII, and C (mg/L) is the concentration after photocatalytic reaction at different time. The photocatalytic experiments of the pure TiO_2 NPs and Stir-TiO_2/Bi_2O_3 were also carried out in the same way.

Results and discussion

XRD analysis

XRD technique was applied to determine the crystal structures of the three resulting samples, and the XRD patterns are presented in Fig. 1. The diffraction peaks of TiO_2 are detected all over the three samples. Specifically, the peaks at $2\theta = 25.3°$, 36.9°, 37.8°, 38.6°, 48.0°, 53.9°, 55.1°, 62.7°, 68.8°, 70.3° and 75.0° correspond to the standard anatase-TiO_2 diffraction peaks for the (1 0 1), (1 0 3), (0 0 4), (1 1 2), (2 0 0), (1 0 5), (2 1 1), (2 0 4), (1 1 6), (2 2 0) and (2 1 5) lattice planes, respectively. From the XRD curves of the two nanocomposite samples, we can observe that there are nine new diffraction peaks at $2\theta = 27.9°$, 31.8°, 32.7°, 46.2°, 46.9°, 54.3°,

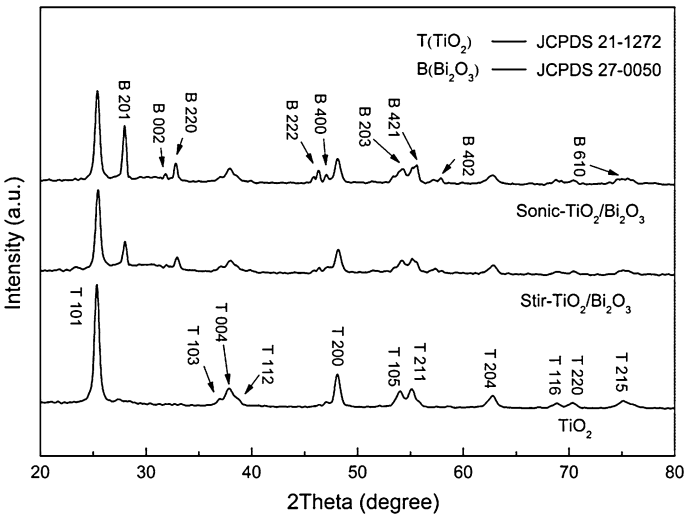

Fig. 1 XRD patterns of Sonic-TiO_2/Bi_2O_3 nanocomposites, Stir-TiO_2/Bi_2O_3 nanocomposites and TiO_2 NPs

55.5°, 57.8° and 74.5°, which are attributed to (2 0 1), (0 0 2), (2 2 0), (2 2 2), (4 0 0), (2 0 3), (4 2 1), (4 0 2) and (6 1 0) facets of β-Bi_2O_3, respectively. These results indicate that the two nanocomposite samples all contain TiO_2 and Bi_2O_3. The three samples are all well crystallized, and no other impure diffraction peaks can be detected in the patterns. It is worth noting that the anatase-TiO2 diffraction peaks of the two nanocomposite samples are weaker than that of pure TiO2 NPs, which can be attributed to the generation of Bi_2O_3. Furthermore, the peaks of Bi_2O_3 become stronger and sharper after ultrasonic treatment, indicating that the Bi_2O_3 in Sonic-TiO_2/Bi_2O_3 have higher crystallinity than that in Stir-TiO_2/Bi_2O_3.

FT-IR analysis

Fourier transform-infrared spectra of two nanocomposite samples and TiO_2 NPs are shown in Fig. 2. The peaks at about 3,750 and 1,552 cm^{-1} are ascribed to unconjugated water [24, 25], while two bands located around 3,440 and 1,643 cm^{-1} can be reasonably assigned to the adsorbed water molecules in the three samples [26, 27]. The FT-IR band at 400–800 cm^{-1} is ascribed to the Ti–O–Ti stretching vibration mode in crystal TiO_2 [28]. The absorption assigned to the SO_4^{2-} has been observed at 1,037 cm^{-1}, which is commonly observed for TiO_2 prepared with titanium oxysulfate hydrate [29]. No significant differences can be observed in the spectra between the three samples, except that a red shift of the Ti–O–Ti bands occurs in the spectrum of Sonic-TiO_2/Bi_2O_3, which might be due to the combination of TiO_2 and Bi_2O_3. This further confirms that the Sonic-TiO_2/Bi_2O_3 is a composite material.

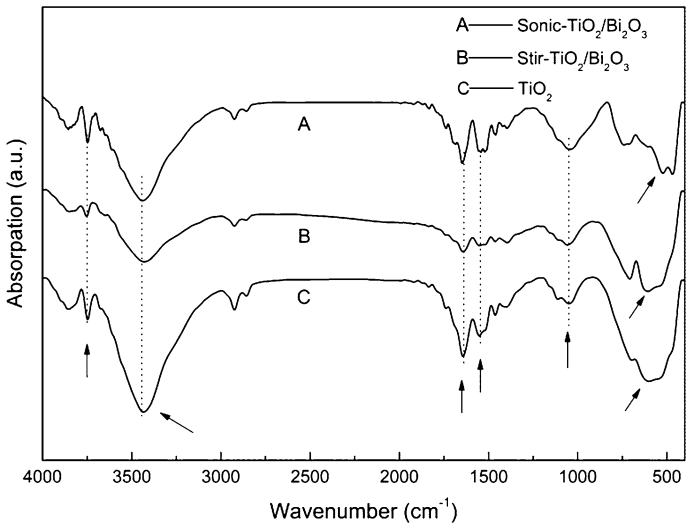

Fig. 2 FT-IR spectra of Sonic-TiO_2/Bi_2O_3 nanocomposites, Stir-TiO_2/Bi_2O_3 nanocomposites and TiO_2 NPs

Morphologies analysis

The morphologies of the samples were characterized to obtain the microstructural information. The FE-SEM images of the TiO_2 NPs, Stir-TiO_2/Bi_2O_3, Sonic-TiO_2/Bi_2O_3 and TEM image of Sonic-TiO_2/Bi_2O_3 nanocomposites are indicated in Fig. 3a–d, respectively. As shown in Fig. 3a, the TiO_2 NPs sample is composed of siamesed massive aggregates which are accumulated from small NPs. Under close observation of these NPs, their diameter range is about 50–100 nm. From Fig. 3b–d, the morphologies of the two nanocomposite samples are also massive aggregates composed of NPs, but the aggregates sizes of them are larger than that of TiO_2 NPs. The serious agglomeration phenomenon can be chalked up to the generation of Bi_2O_3. In comparison, the aggregates sizes of Sonic-TiO_2/Bi_2O_3 are smaller than that of Stir-TiO_2/Bi_2O_3, which indicates that ultrasonic treatment can reduce the agglomeration degree of the TiO_2/Bi_2O_3 nanocomposites.

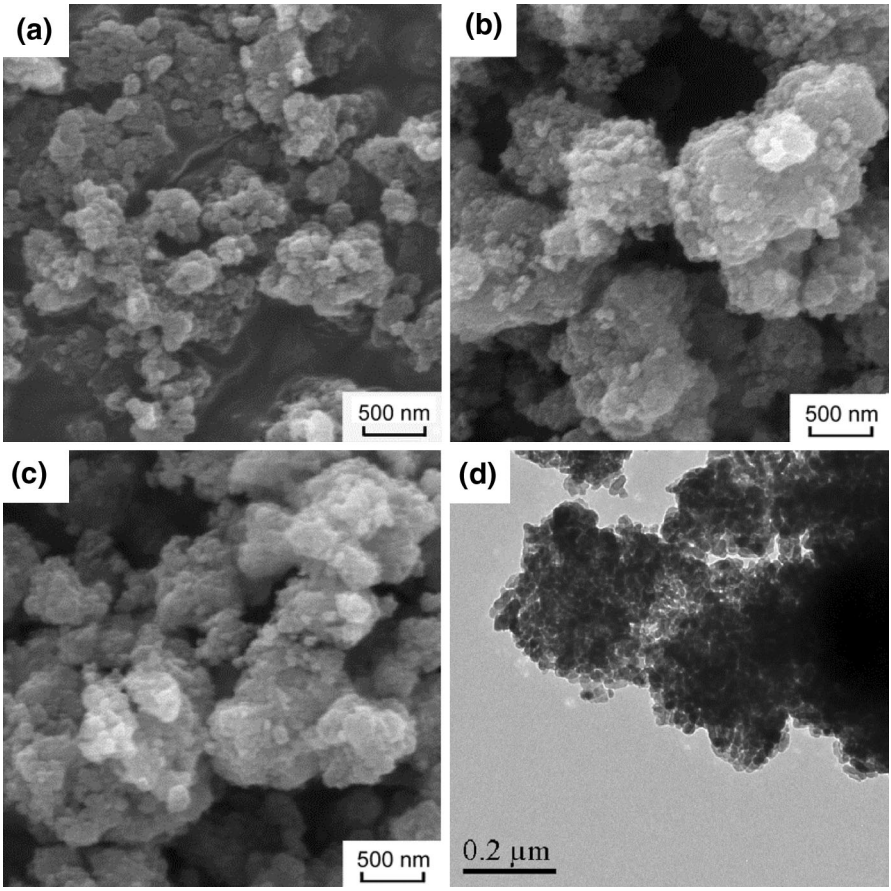

Fig. 3 FE-SEM images of TiO_2 NPs (**a**), Stir-TiO_2/Bi_2O_3 nanocomposites (**b**), Sonic-TiO_2/Bi_2O_3 nanocomposites (**c**), and TEM image of Sonic-TiO_2/Bi_2O_3 nanocomposites (**d**)

EDX analysis

The EDX analysis of the TiO_2 NPs, Stir-TiO_2/Bi_2O_3 and Sonic-TiO_2/Bi_2O_3 nanocomposites are shown in Fig. 4a–c, and the elemental composition tables of the three samples are attached to the figures, respectively. According to the spectroscopies, the TiO_2 NPs contain Ti and O, while two nanocomposite samples all contain Ti, O and Bi. And the two nanocomposite samples have almost the same content of the three elements. These results further testify that the two nanocomposite samples are composed of TiO_2 and Bi_2O_3, which is consistent with the results of XRD and FT-IR analysis.

UV–Vis spectra analysis

The optical absorption properties of the as-obtained samples were measured by a UV–Vis spectrometer, and the UV–Vis absorption spectra for them are shown in Fig. 5. It can be seen that all TiO_2/Bi_2O_3 nanocomposite samples show a spectral response in visible areas owing to the photosensitizing effect of Bi_2O_3. It is well known that photocatalytic reactions are initiated by light, and none of the photocatlysts could work if they cannot absorb light. However, when photocatalysts are illuminated by lights, only a few lights can be absorbed, and most of them have been reflected off. Therefore, the photo-absorption capacity can affect the photocatalytic performances of photocatalytsts [30]. In comparison to Stir-TiO_2/Bi_2O_3, the Sonic-TiO_2/Bi_2O_3 displays higher photo-absorption capacity in the visible region, which might increase its photocatalytic performance. Furthermore, the band gap energies are estimated as 3.19, 3.07 and 2.94 eV for TiO_2 NPs, Stir-TiO_2/Bi_2O_3 and Sonic-TiO_2/Bi_2O_3, respectively, indicating that the Sonic-TiO_2/

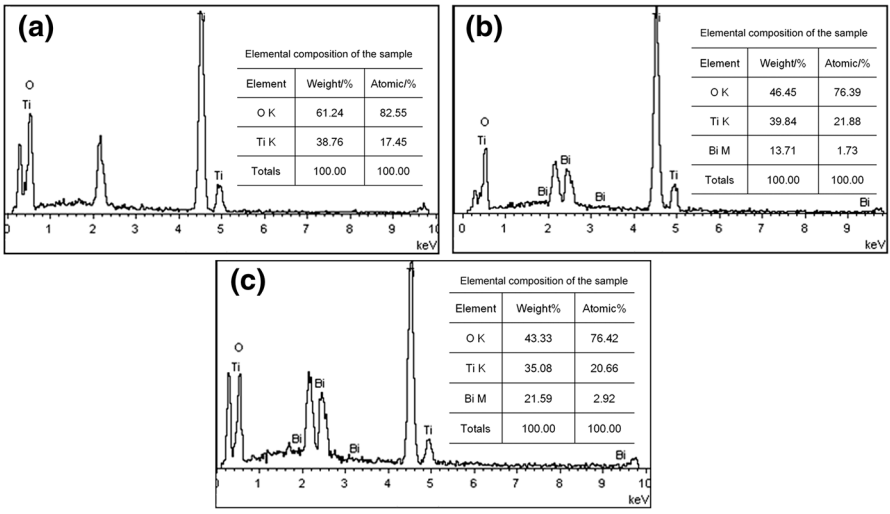

Fig. 4 Energy dispersive spectroscopies of TiO_2 NPs (**a**), Stir-TiO_2/Bi_2O_3 nanocomposites (**b**), and Sonic-TiO_2/Bi_2O_3 nanocomposites (**c**)

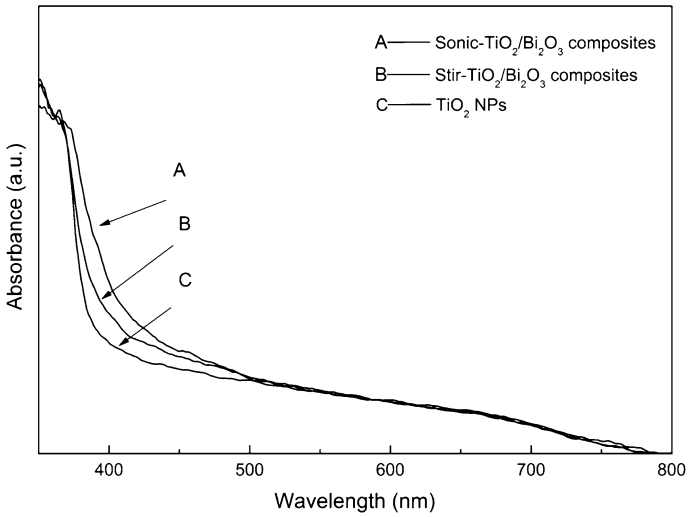

Fig. 5 UV–Visible absorption spectra of Sonic-TiO_2/Bi_2O_3 nanocomposites, Stir-TiO_2/Bi_2O_3 nanocomposites and TiO_2 NPs

Bi_2O_3 can be excited by visible light. The strong visible light absorption capacity and narrow band gap of Sonic-TiO_2/Bi_2O_3 suggests that it should possess excellent visible light photocatalytic activity compared to that of Stir-TiO_2/Bi_2O_3 and TiO_2 NPs [31].

Photocatalytic activities

The photocatalytic activities of TiO_2 NPs, Stir-TiO_2/Bi_2O_3 and Sonic-TiO_2/Bi_2O_3 were evaluated by measuring the photo-degradation of OII aqueous solution (5 mg/L) under visible light irradiation. Figure 6 shows the comparison of the photocatalytic activities between those prepared samples at the same initial condition. After 3 h of visible light irradiation, OII is degraded with different catalysts, but the photocatalytic efficiencies of them are not the same. The TiO_2 NPs exhibit the poorest activity under visible light with only 44.0 % degradation, while the two nanocomposite samples show much higher photocatalytic activities. The photocatalytic efficiency could reach 94.7 % when Sonic-TiO_2/Bi_2O_3 was employed, especially. Furthermore, the blank test shows that the OII degradation is so tiny in the absence of photocatalysts that the self-degradation of OII can be ignored.

The UV–Vis absorption spectra of OII solution after degradation for different times over Sonic-TiO_2/Bi_2O_3 under visible light irradiation were recorded, and are shown in Fig. 7. It can be seen that all of the absorption peaks decrease with the extension of the irradiation time, indicating that the OII molecules have been destroyed in the photocatalytic reaction process [32]. The maximum absorption peak ($\lambda = 485$ nm) decreases gradually and almost completely disappears after 180 min, which suggests that the Sonic-TiO_2/Bi_2O_3 exhibits excellent photocatalytic activity in the decolonization of OII.

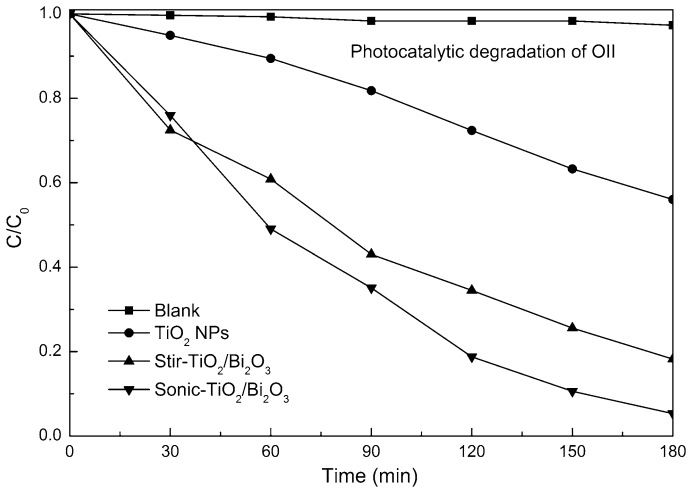

Fig. 6 Photocatalytic degradation of OII using Sonic-TiO_2/Bi_2O_3 nanocomposites, Stir-TiO_2/Bi_2O_3 nanocomposites and TiO_2 NPs under visible light irradiation

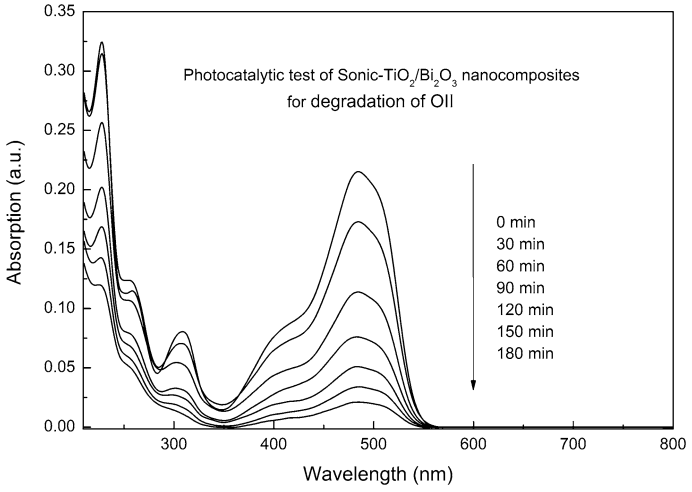

Fig. 7 UV–Vis absorption spectral changes of OII under visible light irradiation using Sonic-TiO_2/Bi_2O_3 nanocomposites

In order to further study the photocatalytic abilities of the prepared samples and the reaction kinetics of OII degradation, the Langmuir–Hinshelwood model [33] has been used here:

$$-\ln\left(\frac{C}{C_0}\right) = kt \tag{2}$$

where k (min^{-1}) is the rate constant value, and t (min) is the reaction time. Figure 8 shows the plot depicting the linear relationship between $-\ln(C/C_0)$ and time for all

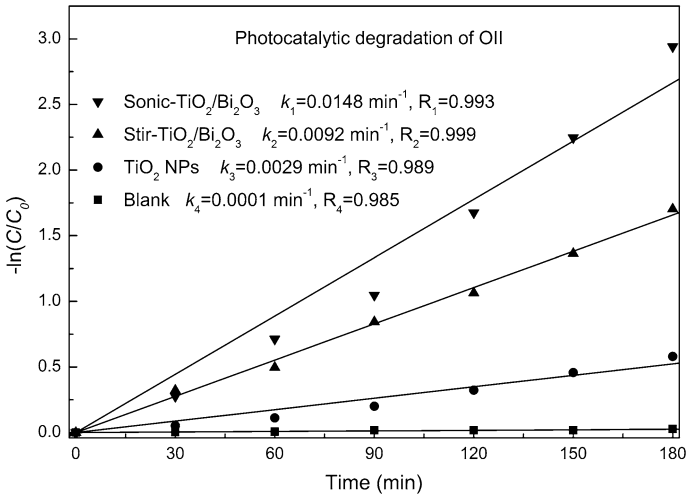

Fig. 8 Kinetics of photocatalytic degradation of OII with Sonic-TiO_2/Bi_2O_3 nanocomposites, Stir-TiO_2/Bi_2O_3 nanocomposites and TiO_2 NPs under UV–Vis irradiation

the samples, while the rate constant values (k) and standard deviation values (R) are also given in the figure. The results show that $-\ln(C/C_0)$ exhibits a good linear relationship with the irradiation time ($R_1 = 0.993$, $R_2 = 0.999$, $R_3 = 0.989$), indicating that the photocatalytic degradation of OII over the three prepared samples follows a first-order kinetic reaction. The rate constant values are determined to be 0.0148 and 0.0092 min^{-1} for Sonic-TiO_2/Bi_2O_3 and Stir-TiO_2/Bi_2O_3, respectively, which are distinctly higher than that of the TiO_2 NPs ($k_3 = 0.0029$ min^{-1}). This fact indicates that the modification with Bi_2O_3 can obviously enhance the photocatalytic activity of TiO_2 under visible light. Furthermore, ultrasonic treatment can even promote the degradation activities of nanocomposite photocatalysts.

Tentative photocatalytic mechanisms

As we all know, TiO_2 is a wide gap (band gap = 3.2 eV) semiconductor, which cannot be activated by visible light, and OII theoretically cannot be decomposed in this system [34]. But the TiO_2 NPs still display 44.0 % degradation yield of OII dye within 180 min, possibly owing to self-sensitization of the OII. As shown in Fig. 9a, the OII molecules adsorbed on the surface of TiO_2 NPs can absorb visible light to produce a singlet and/or triplet state of OII molecules (OII*). The oxidation potential of OII* is more negative than the potential of the conduction band (CB) of TiO_2 NPs, which involves the possibility that electrons would inject into the CB of TiO_2 from OII*. Therefore, the OII is converted to the cationic dye radical, and the injected electrons can take part in the degradation reactions of the pollutants. As a result, the OII molecules have been decomposed in this TiO_2–OII system [35].

When TiO_2 was modified with Bi_2O_3, the photocatalytic mechanisms become much more complex, which can be classified into two reasonable paths. As shown

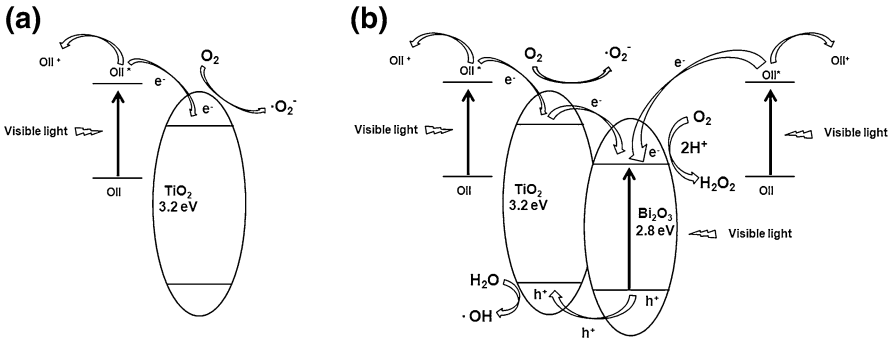

Fig. 9 Schematic illustration for the photocatalytic process of TiO_2 NPs (**a**), TiO_2/Bi_2O_3 nanocomposites (**b**) under visible light irradiation

in Fig. 9b, one is the OII dye sensitization process, which is similar to the photocatalytic process of pure TiO_2 NPs [35]. Another path is the Bi_2O_3-assisted photocatalytic process. As the band gap of Bi_2O_3 is 2.8 eV, it can be easily excited by visible light to form photogenerated electron–hole pairs, while the electrons and holes could induce a series of reactions to decompose OII [14, 15]. In addition, the CB potential of TiO_2 is more negative than that of Bi_2O_3, while the valence band (VB) of Bi_2O_3 is more positive than that of TiO_2 [36]. Hence, the electrons in the CB of TiO_2 could transfer to the CB of Bi_2O_3, and the holes in the VB of Bi_2O_3 could transfer to the VB of TiO_2. These heterojunctions between Bi_2O_3 and TiO_2 could promote separation of photogenerated charge carriers and could also enhance photocatalytic activity [37].

An ultrasonic wave is a kind of sound wave with high energy [38]. When it was applied in the synthesis of TiO_2/Bi_2O_3 nanocomposites, the high energy could promote the crystallization of the NPs, responsible for the further crystallization process [39]. With the help of ultrasonic treatment, the crystallinity of Bi_2O_3 NPs growing on the surface of TiO_2 would be higher, which is beneficial to the charge transfer. As a result, the Sonic-TiO_2/Bi_2O_3 nanocomposite catalyst exhibits the highest photocatalytic activity among the three samples.

Conclusions

In summary, we have demonstrated a new ultrasonic-assisted chemical precipitation method to prepare TiO_2/Bi_2O_3 nanocomposites (Sonic-TiO_2/Bi_2O_3). XRD, FT-IR, FE-SEM, TEM and EDX results indicate that the Sonic-TiO_2/Bi_2O_3 nanocomposites have been successfully synthesized. Optical absorption property analysis shows that this Sonic-TiO_2/Bi_2O_3 possesses the highest visible light absorption capacity. Furthermore, such Sonic-TiO_2/Bi_2O_3 exhibits higher photocatalytic activity for the degradation of OII dye solution under visible light irradiation than either the pure TiO_2 NPs or the TiO_2/Bi_2O_3 obtained by a conventional precipitation method.

References

1. C.A. Martinez-Huitle, S. Ferro, Chem. Soc. Rev. **35**, 1324–1340 (2006)
2. N. Hudson, A. Baker, D. Reynolds, River Res. Appl. **23**, 631–649 (2007)
3. A. Ahmad, A. Idris, B. Hameed, Desalin. Water Treat. **51**, 2554–2563 (2013)
4. V.O. Abramov, A.V. Abramova, P.P. Keremetin, M.S. Mullakaev, G.B. Vexler, T.J. Mason, Ultrason. Sonochem. **21**, 812–818 (2014)
5. L.M. Nieto, G. Hodaifa, S. Rodríguez, J.A. Giménez, J. Ochando, Chem. Eng. J. **173**, 503–510 (2011)
6. T. Mousanejad, M. Khosravi, S. Tabatabaii, A. Khataee, K. Zare, Res. Chem. Intermed. **40**, 711–722 (2014)
7. T. Zhu, J.S. Chen, X.W. Lou, J. Phys. Chem. C **116**, 6873–6878 (2012)
8. A. Petrella, M. Petrella, G. Boghetich, P. Mastrorilli, V. Petruzzelli, E. Ranieri, D. Petruzzelli, Ind. Eng. Chem. Res. **52**, 2201–2208 (2013)
9. Y.H. Zhao, Appl. Mech. Mater. **416**, 1652–1656 (2013)
10. S.G. Kumar, L.G. Devi, J. Phys. Chem. A **115**, 13211–13241 (2011)
11. Y. Lu, Y. Lin, D. Wang, L. Wang, T. Xie, T. Jiang, Nano Res **4**, 1144–1152 (2011)
12. M. Muruganandham, R. Amutha, G.J. Lee, S.H. Hsieh, J.J. Wu, M. Sillanpää, J. Phys. Chem. C **116**, 12906–12915 (2012)
13. X. Liu, L. Pan, J. Li, K. Yu, Z. Sun, J. Nanosci. Nanotechnol. **13**, 5044–5047 (2013)
14. H.Y. Jiang, J.J. Liu, K. Cheng, W.B. Sun, J. Lin, J. Phys. Chem. C **117**, 20029–20036 (2013)
15. H.Y. Jiang, K. Cheng, J. Lin, Phys. Chem. Chem. Phys. **14**, 12114–12121 (2012)
16. Z.F. Bian, J. Zhu, S.H. Wang, Y. Cao, X.F. Qian, H.X. Li, J. Phys. Chem. C **112**, 6258–6262 (2008)
17. D. Li, Y. Zhang, X. Zhou, S. Guo, J. Hazard. Mater. **258**, 42–49 (2013)
18. Y.N. Huo, X.F. Chen, J. Zhang, G.F. Pan, J.P. Jia, H.X. Li, Appl. Catal. B: Environ. **148**, 550–556 (2014)
19. Y.J. Li, T.P. Cao, C.L. Shao, C.H. Wang, J. Inorg. Mater. **27**, 687–692 (2012)
20. X. Zhao, H.J. Liu, J.H. Qu, Appl. Surf. Sci. **257**, 4621–4624 (2011)
21. Z.F. Bian, J. Zhu, S.H. Wang, Y. Cao, X.F. Qian, H.X. Li, J. Phys. Chem. C **112**, 6258–6262 (2008)
22. A.K. Chakraborty, M.E. Hossain, M.M. Rhaman, K.M.A. Sobahan, J. Environ. Sci. **26**, 458–465 (2014)
23. A. Di Paola, M. Bellardita, L. Palmisano, R. Amadelli, L. Samiolo, Catal. Lett. **143**, 844–852 (2013)
24. K. Chakarova, K. Hadjiivanov, Micropor. Mesopor. Mater. **143**, 180–188 (2011)
25. Y. Cheng, L. An, J. Lan, F. Gao, R.Q. Tan, X.M. Li, G.H. Wang, Mater. Res. Bull. **48**, 4287–4293 (2013)
26. V. Pilla, S.R. de Lima, A.A. Andrade, A.C.A. Silva, N.O. Dantas, Chem. Phys. Lett. **580**, 130–134 (2013)
27. M. Tortorelli, G. Landi, L. Lisi, G. Russo, Micropor. Mesopor. Mater. **200**, 216–224 (2014)
28. G.Z. Liao, S. Chen, X. Quan, Y.B. Zhang, H.M. Zhao, Appl. Catal. B: Environ. **102**, 126–131 (2011)
29. L.L. Chen, Y. Zhai, H.Y. Ding, G.H. Zhou, Y.F. Zhu, D. Hui, Compos. Part B-Eng. **45**, 111–116 (2013)
30. J. Zhu, S. Wang, J. Wang, D. Zhang, H. Li, Appl. Catal. B: Environ. **102**, 120–125 (2011)
31. P. Malathy, K. Vignesh, M. Rajarajan, A. Suganthi, Ceram. Int. **40**, 101–107 (2014)
32. R. Chauhan, A. Kumar, R. Chaudhary, Res. Chem. Intermed. **39**, 645–657 (2013)
33. Z. Liu, B. Wu, Y. Zhao, J. Niu, Y. Zhu, Ceram. Int. **40**, 5597–5603 (2014)
34. Y. Zhang, S. Liu, Z. Xiu, Q. Lu, H. Sun, G. Liu, J. Nanopart. Res. **16**, 1–9 (2014)
35. Y. Bessekhouad, N. Chaoui, M. Trzpit, N. Ghazzal, D. Robert, J.V. Weber, J. Photochem. Photobiol. A: Chem. **183**, 218–224 (2006)
36. J. Hou, C. Yang, Z. Wang, S. Jiao, H. Zhu, Appl. Catal. B: Environ. **129**, 333–341 (2013)
37. J. Chen, S. Qin, Y. Liu, F. Xin, X. Yin, Res. Chem. Intermed. **40**, 637–648 (2014)
38. K. Ullah, L. Zhu, Z.D. Meng, S. Ye, S. Sarkar, W.C. Oh, J. Mater. Sci. **49**, 4139–4147 (2014)
39. L. Zhou, W. Wang, L. Zhang, J. Mol. Catal. A: Chem. **268**, 195–200 (2007)